

Time-dependent transport of electrons through a photon cavity

Vidar Gudmundsson,^{1,*} Olafur Jonasson,¹ Chi-Shung Tang,^{2,†} Hsi-Sheng Goan,^{3,4,‡} and Andrei Manolescu⁵

¹*Science Institute, University of Iceland, Dunhaga 3, IS-107 Reykjavik, Iceland*

²*Department of Mechanical Engineering, National United University, 1, Lienda, Miaoli 36003, Taiwan*

³*Department of Physics and Center for Theoretical Sciences,
National Taiwan University, Taipei 10617, Taiwan*

⁴*Center for Quantum Science and Engineering, National Taiwan University, Taipei 10617, Taiwan*

⁵*Reykjavik University, School of Science and Engineering, Menntavegur 1, IS-101 Reykjavik, Iceland*

We use a non-Markovian master equation to describe the transport of Coulomb interacting electrons through an electromagnetic cavity with one quantized photon mode. The central system is a finite parabolic quantum wire that is coupled weakly to external parabolic quasi-one-dimensional leads at $t = 0$. With a stepwise introduction of complexity to the description of the system and a corresponding stepwise truncation of the ensuing many-body spaces we are able to describe the time-dependent transport of Coulomb-interacting electrons through a geometrically complex central system. We take into account the full electromagnetic interaction of electrons and cavity photons without resorting to the rotating wave approximation or reduction of the electron states to two levels. We observe that the number of initial cavity photons and their polarization can have important effects on the transport properties of the system. The quasiparticles formed in the central system have a lifetime limited by the coupling to the leads and radiation processes active on a much longer timescale.

PACS numbers: 73.23.-b, 78.67.-n, 42.50.Pq, 73.21.Hb

I. INTRODUCTION

During the past decade there has been increasing interest in exploring time-dependent quantum transport through open mesoscopic systems in a strong system-lead coupling regime.¹⁻⁷ Utilizing the tunable dynamic response of transient time-dependent transport enables development of switchable mesoscale electronic devices, in which the interplay of the mesoscopic system with external perturbations plays an important role.⁸⁻¹²

In the weak system-lead coupling regime, the wide-band and the Markovian approximation are usually employed, by neglecting the energy dependence of the electron tunneling rate, as well as memory effects in the system, respectively.¹³⁻¹⁵ It is assumed that the correlation time of the electrons in the leads is much shorter than the typical response time of the central system. However, transient transport properties, which are intrinsically linked to coherence and relaxation dynamics, cannot generally be described in the Markovian limit. One has to take into account the energy-dependent spectral density in the leads, and an accurate numerical method for such a nonequilibrium transient time-dependent transport is desirable. A non-Markovian density-matrix formalism involving the energy dependent coupling elements should be considered based on the generalized master equation (GME).¹⁶⁻²¹ How to appropriately describe the carrier quantum dynamics under nonequilibrium conditions in realistic device geometries is a challenging problem.^{10,20,22}

More recently, manipulation of the electron-photon coupled quantum systems in an electromagnetic cavity has become one of the key issues to be implemented in quantum information processing devices. Utilizing

the giant dipole moments of intersubband transitions in quantum wells^{23,24} enables researchers to reach the ultrastrong electron-photon coupling regime.²⁵⁻²⁷ In this regime, the dynamical electron-photon coupling mechanism has to be explored beyond the wide-band and rotating-wave approximations.²⁸⁻³⁰ Nevertheless, the dynamical time-dependent transport of Coulomb interacting electrons in a specified geometry through an electromagnetic cavity with quantized photon modes remains unexplored.

In the present work, we explore the electronic transient transport dynamics of an open quantum wire placed in a linearly polarized electromagnetic field created in a cavity.^{31,32} The wire is contacted to two quasi-one-dimensional (Q1D) semi-infinite leads. A bias voltage is suddenly switched on between the leads, along the wire. The whole structure is considered to be placed in a perpendicular homogeneous external magnetic field. We use the Nakajima-Zwanzig (N-Z) formalism to project the time evolution of the system onto the Hilbert space of the central element (the short wire) by taking trace with respect to the operators in the leads.^{33,34} The transient transport properties will be explored by calculating the time-dependent total mean number of electrons and photons, and the time-dependent total charge current from the left (L) lead to the right (R) lead.

The paper is organized as follows. In Sec. II, we shall describe our theoretical model including the electron system in an electromagnetic cavity by coupling a many-level electron system with photons using a full photon energy spectrum of a single cavity mode in the Fock space. The N-Z framework is utilized to describe the system-lead coupling.^{33,34} In section III we investigate the dynamical transient transport properties. Concluding remarks will

be presented in Sec. IV.

II. MODEL

We start by describing a Coulomb interacting electron system in a closed finite system in an electromagnetic cavity with quantized photon modes of two different polarizations. Later we shall open the system by coupling it to external Q1D leads in order to allow for transport of electrons through it. In the closed system the number of electrons is constant, but in order to accomplish the opening up of the system we need to calculate its equilibrium properties for a variable number of electrons. In the equilibrium and transport calculation to follow N_{SES} will represent the number of Single-Electron States (SESs) used to build the Many-Electron States (MESs) of the system.^{19,20}

A. Electron system in an electromagnetic cavity

The central element, a short wire placed in the x - y plane is in an external homogeneous classical magnetic field constant in time, $\mathbf{B} = B\hat{\mathbf{z}}$, introduced by the vector potential \mathbf{A}_{ext} , and cavity fields represented by a quantized vector field \mathbf{A} . The many-body Hamiltonian of this closed system is

$$\begin{aligned}
H_0 &= H_{\text{Coul}} + H_{\text{EM}} \\
&+ \int d\mathbf{r} \psi^\dagger \left\{ \frac{1}{2m^*} \left(\mathbf{p} + \frac{e}{c} [\mathbf{A}_{\text{ext}} + \mathbf{A}] \right)^2 + \frac{1}{2} m^* \Omega_0^2 y^2 \right\} \psi \\
&= \int d\mathbf{r} \psi^\dagger \left\{ \frac{1}{2m^*} \left(\mathbf{p} + \frac{e}{c} \mathbf{A}_{\text{ext}} \right)^2 + \frac{1}{2} m^* \Omega_0^2 y^2 \right\} \psi \\
&+ H_{\text{Coul}} + H_{\text{EM}} - \frac{1}{c} \int d\mathbf{r} \mathbf{j} \cdot \mathbf{A} - \frac{e}{2m^*c^2} \int d\mathbf{r} \rho A^2 \\
&= \int d\mathbf{r} \psi^\dagger \left\{ \frac{\pi^2}{2m^*} + \frac{1}{2} m^* \Omega_0^2 y^2 \right\} \psi + H_{\text{Coul}} + H_{\text{EM}} \\
&- \frac{1}{c} \int d\mathbf{r} \mathbf{j} \cdot \mathbf{A} - \frac{e}{2m^*c^2} \int d\mathbf{r} \rho A^2, \quad (1)
\end{aligned}$$

with H_{Coul} the Hamiltonian for the Coulomb interaction of the electrons and H_{EM} the Hamiltonian of the cavity photons to be introduced later and the charge current density and charge density

$$\mathbf{j} = -\frac{e}{2m^*} \{ \psi^\dagger (\boldsymbol{\pi} \psi) + (\boldsymbol{\pi}^* \psi^\dagger) \psi \}, \quad \rho = -e\psi^\dagger \psi, \quad (2)$$

where

$$\boldsymbol{\pi} = \left(\mathbf{p} + \frac{e}{c} \mathbf{A}_{\text{ext}} \right). \quad (3)$$

The static magnetic field $\mathbf{B} = \nabla \times \mathbf{A}_{\text{ext}}$ together with the parabolic confinement of the q-1DES introduce a characteristic length $a_w = \sqrt{\hbar/(m^*\Omega_w)}$, with $\Omega_w^2 = \omega_c^2 + \Omega_0^2$ and the cyclotron frequency $\omega_c = eB/(m^*c)$. The frequency

Ω_0 characterizes the strength of the electron confinement in the y -direction. The finite parabolic quantum wire has length L_x and hard walls at $x = \pm L_x/2$.

In terms of creation and annihilation operators the Hamiltonian of the closed system takes the form

$$\begin{aligned}
H_0 &= H_e + H_{\text{EM}} + H_{\text{Coul}} + H_{e-\text{EM}} \\
&= \sum_i E_i d_i^\dagger d_i + \hbar\omega a^\dagger a + \frac{1}{2} \sum_{ijrs} \langle ij | V_{\text{Coul}} | rs \rangle d_i^\dagger d_j^\dagger d_s d_r \\
&+ \mathcal{E}_c \sum_{ij} d_i^\dagger d_j g_{ij} \{ a + a^\dagger \} \\
&+ \mathcal{E}_c \left(\frac{\mathcal{E}_c}{\hbar\Omega_w} \right) \sum_i d_i^\dagger d_i \left\{ \left(a^\dagger a + \frac{1}{2} \right) + \frac{1}{2} (aa + a^\dagger a^\dagger) \right\}, \quad (4)
\end{aligned}$$

where the single-electron states (SESs) of the closed system are labeled with Latin indices, $\{i, j, r, s\}$, a is the destruction operator of one quantum of the single-mode cavity field with frequency ω , and d_i is an annihilation operator of the non-interacting single-electron state $|i\rangle$ with energy E_i .

The electromagnetic cavity is a rectangular box $(x, y, z) \in \{[-a_c/2, a_c/2] \times [-a_c/2, a_c/2] \times [-d_c/2, d_c/2]\}$ with the finite quantum wire centered in the $z = 0$ plane. The polarization of the electric field can be chosen along the transport direction, x , or perpendicular to it by selecting the TE_{011} or the TE_{101} mode, respectively. In the Coulomb gauge the vector field is then

$$\mathbf{A}(\mathbf{r}) = \begin{pmatrix} \hat{\mathbf{e}}_x \\ \hat{\mathbf{e}}_y \end{pmatrix} \mathcal{A} \{ a + a^\dagger \} \begin{pmatrix} \cos\left(\frac{\pi x}{a_c}\right) \\ \cos\left(\frac{\pi y}{a_c}\right) \end{pmatrix} \cos\left(\frac{\pi z}{d_c}\right), \quad (5)$$

with the upper equation representing the TE_{011} mode and the lower one for TE_{101} .

The effective dimensionless coupling tensor of the electrons to the cavity mode due to the linear term in \mathbf{A} in Eq. (1) is

$$\begin{aligned}
g_{ij} &= \frac{a_w}{2\hbar} \int d\mathbf{r} [\psi_i^*(\mathbf{r}) \{ (\hat{\mathbf{e}} \cdot \boldsymbol{\pi}) \psi_j(\mathbf{r}) \} \\
&+ \{ (\hat{\mathbf{e}} \cdot \boldsymbol{\pi}) \psi_i(\mathbf{r}) \}^* \psi_j(\mathbf{r})], \quad (6)
\end{aligned}$$

since we have introduced the characteristic energy scale $\mathcal{E}_c = e\mathcal{A}\Omega_w a_w/c = g^{\text{EM}}$ for the electron-cavity photon coupling. In the calculation of the energy spectrum of the electron-photon Hamiltonian (4) we will retain all resonant and antiresonant terms in the photon creation and annihilation operators and not use the rotating wave approximation, but in the calculations of the electron-photon coupling tensor (6) we assume $a_w, L_x \ll a_c$ and approximate $\cos(\pi\{x, y\}/a_c) \sim 1$ in Eq. (5) for the cavity vector field \mathbf{A} .

After the construction of the Fock space $\{|\alpha\rangle\}$ with the SESs that will later be deemed as relevant to the electron transport an exact numerical diagonalization is used to obtain the Coulomb interacting MESs $\{|\mu\rangle\}$ with the

energy spectrum \tilde{E}_μ and the unitary transformation^{22,35}

$$|\mu\rangle = \sum_{\alpha} \mathcal{V}_{\mu\alpha} |\alpha\rangle. \quad (7)$$

The total Hamiltonian of the electrons and the cavity fields can then be written in terms of the interacting MESs

$$\begin{aligned} H_0 = & \sum_{\mu} |\mu\rangle \tilde{E}_{\mu} \langle\mu| + \hbar\omega a^{\dagger} a \\ & + \mathcal{E}_c \sum_{\mu\nu ij} |\mu\rangle \langle\mu| \mathcal{V}^{\dagger} d_i^{\dagger} d_j \mathcal{V} |\nu\rangle \langle\nu| g_{ij} \{a + a^{\dagger}\} \\ & + \mathcal{E}_c \left(\frac{\mathcal{E}_c}{\hbar\Omega_w} \right) \sum_{\mu\nu i} |\mu\rangle \langle\mu| \mathcal{V}^{\dagger} d_i^{\dagger} d_i \mathcal{V} |\nu\rangle \langle\nu| \\ & \left\{ \left(a^{\dagger} a + \frac{1}{2} \right) + \frac{1}{2} (aa + a^{\dagger} a^{\dagger}) \right\} \quad (8) \end{aligned}$$

and its energy spectrum has to be sought in a Fock space constructed from the space of the Coulomb interacting MESs $\{|\alpha\rangle\}$ and the Fock space of photons $\{|N_{\text{ph}}\rangle\}$

$$|\alpha\rangle \otimes |N_{\text{ph}}\rangle \longrightarrow |\alpha\rangle_{\text{e-EM}}. \quad (9)$$

The diagonalization of the electron-photon Hamiltonian (4) yields

$$|\tilde{\mu}\rangle = \sum_{\alpha} \mathcal{W}_{\mu\alpha} |\alpha\rangle_{\text{e-EM}}. \quad (10)$$

The general scheme here is to start the numerical calculations with a fairly large number of SESs, N_{SES} , and retain only a certain number of MESs in the energy range that is relevant to the transport later, because the total number of MESs, N_{MES} , may be too large for the subsequent calculations. We will call a further twist on this procedure: ‘‘A stepwise introduction of complexity to the model and a stepwise truncation of its many-body space’’. First, we introduce the Coulomb interaction between the electrons, second, we truncate the huge many-electron space. Then we add the Hamiltonian of photons and the electron-photon interaction, and again undertake a truncation of the many-body space in order to have a number of Many Body States (MBSs) for which the transport calculation can be performed. The MBSs are eigenstates of the interacting electron-photon system. We stress here that the unitary transformations necessary between the different many-body spaces, Eqs (7) and (10), have to be completed before truncation. In actual numbers, in the transport calculations here for $g^{\text{EM}} = \mathcal{E}_c \leq 0.1$ meV we used 10 SESs resulting in 1024 MBSs. The Fock-space of Coulomb interacting electrons was then truncated to the lowest 64 states. The inclusion of the single photon mode was accomplished with 27 photon states and the ensuing 1728 photon-electron many-body states will be truncated to the 64 states lowest in energy before the onset of the transport calculation. In order to present the energy spectra for the closed electron-photon system in

Fig. 1 we use 200 electron states and 20 photon states for the much larger values of the coupling g^{EM} . For the closed system we calculate the energy-spectra for each number of electrons present separately. We present the calculations for the closed system in a separate publication with more details on the convergence of the calculations and properties of the system for high values of the coupling constant.³⁶ There we also discuss when the second order term in \mathbf{A} in the electron-photon interaction is necessary for our model of a finite quantum wire.

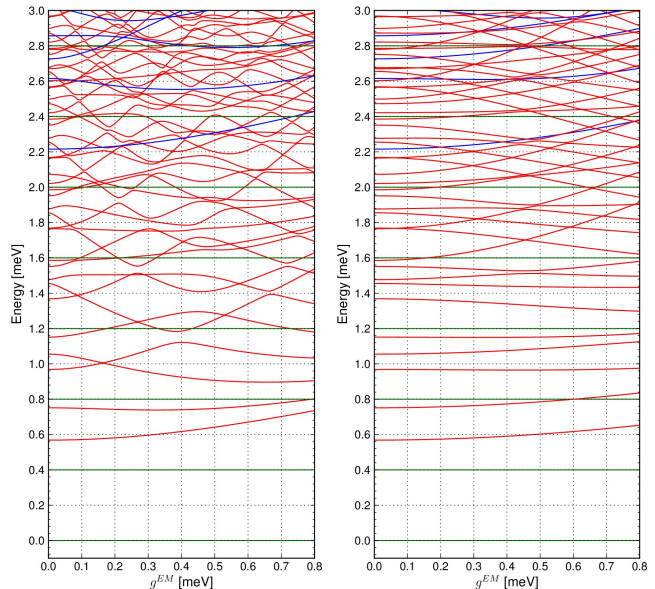


FIG. 1. (Color online) The many-body energy spectra for Coulomb interacting electrons coupled to quantized cavity photon modes with the electric component polarized along the finite quantum wire (x-polarization, left panel), and perpendicular to the wire (y-polarization, right panel) versus the electron-photon coupling strength $g^{\text{EM}} = \mathcal{E}_c$. In the energy range shown there are states with no electrons (green), one electron (red), and two electrons (blue). $B = 0.1$ T, $\hbar\Omega_0 = 1.0$ meV, $\hbar\omega = 0.4$ meV, $L_x = 300$ nm, $m^* = 0.067m_e$, $\kappa = 12.4$, the dielectric constant of GaAs.

The many-body energy spectrum of the electron-photon states are shown in Fig. 1 for the two polarizations, along the finite quantum wire (x-polarization) and perpendicular to it (y-polarization). The horizontal states (green) in Fig. 1 are states only with photons and no electrons that are thus independent of the coupling of the electrons and the photons.

In order to gain further insight into the character of the many-body states in Fig. 1 we plot in Fig. 2 the number of electrons in each state $|\tilde{\mu}\rangle$, a conserved quantity, and thus an integer. In the same plot we add the diagonal of the photon number operator $N_{\text{ph}} = a^{\dagger}a$ in the appropriate space $\{|\tilde{\mu}\rangle\}$. The photon number is not a conserved quantity in the closed system, but the diagonal of the operator should give us some indication of the strong mixing of the photon-electron states by the cavity

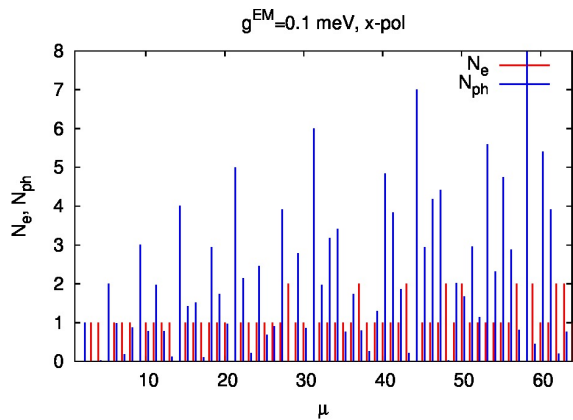


FIG. 2. (Color online) The number of electrons in the many-body state $|\mu\rangle$ (red), and the diagonal element of the photon-number operator, $N_{\mu\mu}^{\text{ph}}$ (blue). $B = 0.1$ T, $g^{\text{EM}} = 0.1$ meV, $\hbar\Omega_0 = 1.0$ meV, $\hbar\omega = 0.4$ meV, $L_x = 300$ nm, $m^* = 0.067m_e$, $\kappa = 12.4$.

coupling. Indeed, we see a considerable photon content in many states, not only the few ones that contain no electrons (i.e. $\mu = 1, 2, 5, 9, 14, 21, 31, 44, 58$).

The spectra versus the coupling constant g^{EM} in Fig. 1 have resemblance with the energy spectrum of a single electron versus the magnetic field B in a non-circular quantum dot.^{37,38} The reason comes clear when the single-electron Hamiltonian for the electron is written in terms of lowering and raising operators and compared to the many-body e-EM Hamiltonian (4). As long as the A^2 -term is included the magnetic field in the dot, B , and the coupling to the photons, g^{EM} , in our model play a similar role. The xy -symmetry breaking is not only caused by the geometry of the central system here, but also by the polarization of the photon field.

Here, we have coupled a many-level electron system with photons using the full electromagnetic coupling (8), and it is interesting to compare the results with spectra obtained for the Jaynes-Cummings model without the rotating wave approximation derived by Feranchuk et al.³⁹ and Li et al.⁴⁰ This comparison will be detailed in another publication concentrated on the properties of the closed system.³⁶

B. System connected to leads

The closed system of Coulomb interacting electrons interacting with the single electromagnetic cavity mode is coupled at $t = 0$ to external leads acting as electron reservoirs. We use a formalism proposed by Nakajima and Zwanzig to project the time evolution of the system onto the central system by partial tracing operations with respect to the operators of the leads.^{33,34} The coupling Hamiltonian is of the form

$$H_{\text{T}}(t) = \sum_{i,l} \chi^l(t) \int dq \left\{ T_{qi}^l c_{ql}^\dagger d_i + (T_{qa}^l)^* d_i^\dagger c_{ql} \right\}, \quad (11)$$

where $l = \{L, R\}$ referring to the left and the right lead, and $\chi^l(t)$ is the time-dependent switching function of the coupling. The semi-infinite leads are in the same perpendicular constant external magnetic field \mathbf{B} as the central system. Their energy spectra are continuous bands and the integral in Eq. (11) represents a summation over the band index and an integral over the continuous ‘‘momentum’’ q from the band bottom to an appropriate band cut-off. The coupling tensor T_{qi}^l of a single-electron states $|q\rangle$ in the lead l to states $|i\rangle$ in the system is modeled as a non-local overlap integral of the corresponding wave functions in the contact regions of the system, Ω_S^l , and the lead l , Ω_l ²⁰

$$T_{iq}^l = \int_{\Omega_S^l \times \Omega_l} d\mathbf{r} d\mathbf{r}' [\psi_q^l(\mathbf{r}')]^* \psi_i^S(\mathbf{r}) g_{iq}^l(\mathbf{r}, \mathbf{r}'). \quad (12)$$

The function

$$g_{iq}^l(\mathbf{r}, \mathbf{r}') = g_0^l \exp[-\delta_1^l(x-x')^2 - \delta_2^l(y-y')^2] \times \exp\left(\frac{-|E_i - \epsilon^l(q)|}{\Delta_E^l}\right). \quad (13)$$

with $\mathbf{r} \in \Omega_S^l$ and $\mathbf{r}' \in \Omega_l$ defines the ‘nonlocal overlap’ and their affinity in energy.

The Liouville-von Neumann equation describing the time-evolution of the total system, the finite quantum wire, the cavity photons, and the leads

$$i\hbar\dot{W}(t) = [H(t), W(t)], \quad W(t < 0) = \rho_L \rho_R \rho_S, \quad (14)$$

where W is the statistical operator of the total system and the equilibrium density operator of the disconnected lead $l \in \{L, R\}$ with chemical potential μ_l is

$$\rho_l = \frac{e^{-\beta(H_l - \mu_l N_l)}}{\text{Tr}_l\{e^{-\beta(H_l - \mu_l N_l)}\}}. \quad (15)$$

Commonly, the spectral density $J_a(\omega)$ is used to describe the coupling of states in an open system to reservoirs or leads.^{12,41} We do not use it explicitly here, but the spectral density for lead l with respect to the SES a in the central system

$$J_i^l(E) \propto \int dq |T_{iq}^l|^2 \delta(E - \epsilon^l(q)) \quad (16)$$

is a convenient tool to demonstrate graphically the phenomenological coupling selected here, in Equations (12) and (13). In order to do this we show first in Fig. 3 the single-electron energy spectrum in the leads and in Fig. 4 the spectral density $J_i^l(E)$ and the probability density for each SES used to build the MESSs of the system. We see in Fig. 4 from jumps in the spectral density that SESs belonging to different subbands in the central system have different coupling strengths to the subbands in the leads as a result of their symmetry. The simple geometry of the central system here does not result in states with widely different localization character.

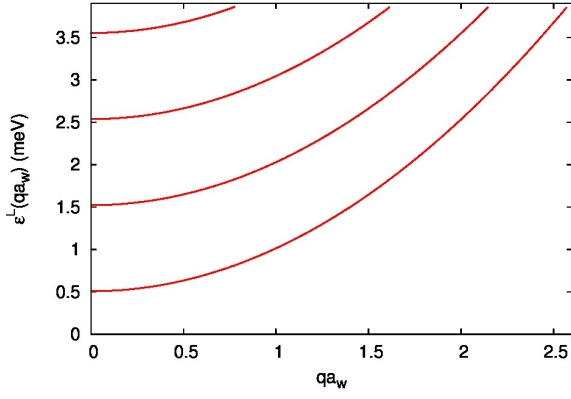


FIG. 3. The single electron energy spectrum of the leads. $B = 0.1$ T, $\hbar\Omega_0^l = 1.0$ meV.

The Liouville-von Neumann equation is projected on the central system of electrons and photons by partial tracing operations with respect to the operators of the leads. Defining the reduced density operator (RDO) of the central system

$$\rho_S(t) = \text{Tr}_L \text{Tr}_R W(t), \quad \rho_S(0) = \rho_S, \quad (17)$$

we obtain an integro-differential equation for the RDO, the generalized master equation (GME)

$$\begin{aligned} \dot{\rho}_S(t) = & \frac{i}{\hbar} [H_S, \rho_S(t)] \\ & - \frac{1}{\hbar^2} \text{Tr}_{\text{res}} \left\{ \left[H_T(t'), \int_0^t dt' [U(t-t')H_T(t')U^+(t-t') \right. \right. \\ & \left. \left. , U_0(t-t')\rho_S(t')U_0^+(t-t') \right] \right\}, \quad (18) \end{aligned}$$

with the time evolution operator for the isolated systems of Coulomb interacting electrons interacting with photons, and noninteracting electrons in the leads, $U(t) = \exp\{-i(H_e + H_{\text{Coul}} + H_{\text{EM}} + H_L + H_R)t/\hbar\}$, without the coupling $H_T(t)$. The time evolution of the closed isolated system of Coulomb interacting electrons interacting with the photons is governed by $U_0(t) = \exp\{-iH_0t/\hbar\}$.

The equation for the RDO (18) can be cast into a coupled set of integro-differential equations for the matrix elements of the RDO by projecting it on the $\{|\check{\mu}\rangle\}$ -basis in a similar manner as was done for the Coulomb interacting electrons in our former work without photons.^{22,35} The kernel of the equation of motion for the RDO (18) has been approximated to the second order for the lead-system coupling $H_T(t)$, but due to the integral structure of the equation the coupling is present in the solution to higher order.

It is convenient to express many operators of the system in a particular basis, i. e. like the basis $\{|\mu\rangle\}$ of independent electrons, or in the Coulomb interacting basis before coupling to the photons $\{|\mu\rangle\}$. The time-dependent mean values of these operators are best calculated by employing a unitary transformation between

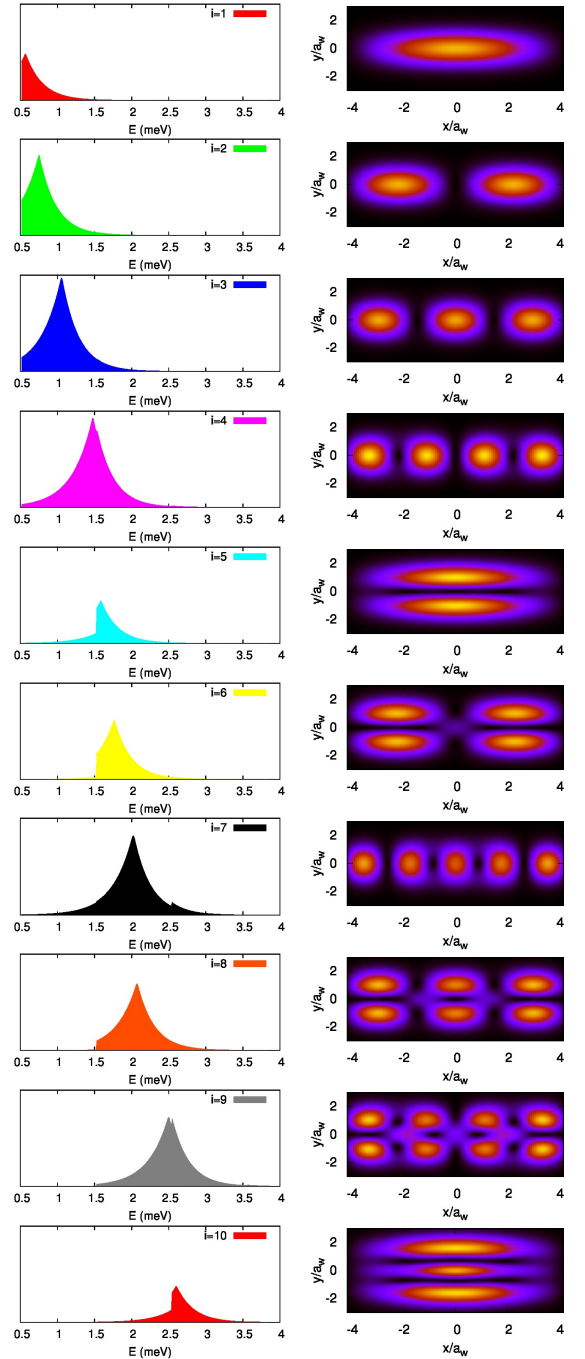


FIG. 4. (Color online) The spectral density $J_i^l(E)$ (left) and the probability amplitude for the corresponding single-electron eigenstate (right). $B = 0.1$ T, $\hbar\Omega_0^l = 1.0$ meV, $L_x = 300$ nm, $\Delta_E^l = 0.25$ meV, $g_0^l a_w^{3/2} = 53.14$ meV, $\delta_{1,2}^l a_w^2 = 0.4916$.

the bases. The photon number operator $N_{\text{ph}} = a^\dagger a$ is best constructed in the $\{|\mu\rangle_{e\text{-EM}}\}$ -basis, and the unitary

transform introduced in Eq. (10) to the $\{|\check{\mu}\rangle\}$ -basis yields

$$\begin{aligned} \langle a^\dagger a \rangle_{e-\text{EM}} &= \sum_{\mu} \langle \check{\mu} | \rho(t) a^\dagger a | \check{\mu} \rangle \\ &= \text{Tr}_S \{ \rho(t) \mathcal{W}^\dagger N_{\text{ph}} \mathcal{W} \}. \end{aligned} \quad (19)$$

Just as a reminder, the unitary transform is performed before the basis is truncated to the size of the matrix representing the RDO in the $\{|\check{\mu}\rangle\}$ -basis dictated by the computational effort in solving the GME (18).

The time-dependent average current J_T^L into the system from the left lead, and J_T^R from the system into the right lead are calculated from the GME (18) along directions introduced in earlier publications.^{19,20,35}

III. TRANSPORT PROPERTIES

For a smooth coupling of the left and the right leads to the central system of electrons and photons we use a switching function (12)

$$\chi^l(t) = \left(1 - \frac{2}{e^{\alpha^l t} + 1} \right), \quad l \in \{L, R\} \quad (20)$$

with $\alpha^l = 0.2 \text{ ps}^{-1}$. We fix the temperature of the reservoirs at $T = 0.5 \text{ K}$, and the coupling strength as $g_0^l a_w^{3/2} = 53.14 \text{ meV}$. We select a bias over the central system by specifying $\mu_L = 2.0 \text{ meV}$, and $\mu_R = 1.4 \text{ meV}$.

The time-evolution of the total mean number of electrons $\langle N_e(t) \rangle$ is displayed in Fig. 5 for two values of the electron-photon coupling g^{EM} . Initially, no electron is present in the central system, but an integer number of photons is specified with a given polarization. For the weaker coupling, $g^{\text{EM}} = 0.01 \text{ meV}$, the charging of the central system seems to be rather independent of the initial number of cavity photons present and their polarization. Well after the charging, ($t \sim 300 \text{ ps}$), a slight difference in the total charge as a function of the initial condition can be observed, but it is very similar to the difference seen for higher coupling, $g^{\text{EM}} = 0.1 \text{ meV}$. More interestingly, the charging is influenced by the initial photon number and their polarization for the higher electron-photon coupling. The charging is slowed down by a higher number of x-polarized photons. The total number of electrons in the system does not exceed one as could be expected by comparing the values of the chemical potentials in the leads and the energy spectral in Fig. 1, we are in the Coulomb-blocking regime.

For the parameters chosen here describing the geometry and the potentials describing the central system the aspect ratio of the system for the low energy range is such that states that can be associated with motion in the x -direction are more numerous than states describing motion in the y -direction as can be verified by a glance at the lowest 10 eigenstates shown in Fig. 4. We should also have in mind that the photon energy $\hbar\omega = 0.4 \text{ meV} < \hbar\Omega_0 = 1.0 \text{ meV}$, the characteristic energy for parabolic confinement in the y -direction.

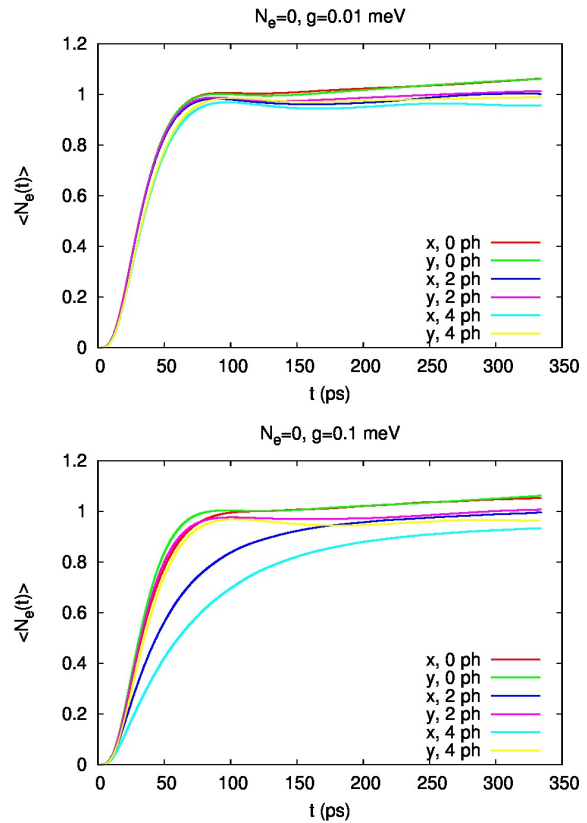


FIG. 5. (Color online) The total mean number of electrons $\langle N_e(t) \rangle$ as a function of time for $g^{\text{EM}} = 0.01 \text{ meV}$ (upper panel) and $g^{\text{EM}} = 0.10 \text{ meV}$ (lower panel). $B = 0.1 \text{ T}$, $\hbar\Omega_0 = 1.0 \text{ meV}$, $L_x = 300 \text{ nm}$, $\hbar\omega = 0.4 \text{ meV}$, $\mu_L = 2.0 \text{ meV}$, $\mu_R = 1.4 \text{ meV}$, $\Delta_E^l = 0.25 \text{ meV}$, $g_0^l a_w^{3/2} = 53.14 \text{ meV}$, $\delta_{1,2}^l a_w^2 = 0.4916$, $m^* = 0.067m_e$, and $\kappa = 12.4$.

A clearer picture of the charging phenomena can be obtained by observing not the total amount of charge, but the time-dependent charging of the individual MBSs that are included in our calculation. This information is presented in Fig. 6 for the weaker electron-photon coupling, and in Fig. 7 for the stronger one.

We immediately notice that in the case of the weaker coupling, Fig. 6, the occupation of the MBSs is almost independent of the polarization of the cavity photons, but as could be expected a higher number of them initially present promotes the occupation of higher energy states. The occupation of the MBSs for 4 initial photons is indicative of a system strongly out of equilibrium with some lower lying MBSs almost empty.

In the case of the stronger electron-photon coupling the occupation of the MBSs is still similar to the results for the weaker coupling for the y -polarization, but a drastic change is visible for the x -polarization with more MBSs partially occupied.

In order to analyze the effects of different number of photons on the charging of the central system we show first the time-evolution of the total mean num-

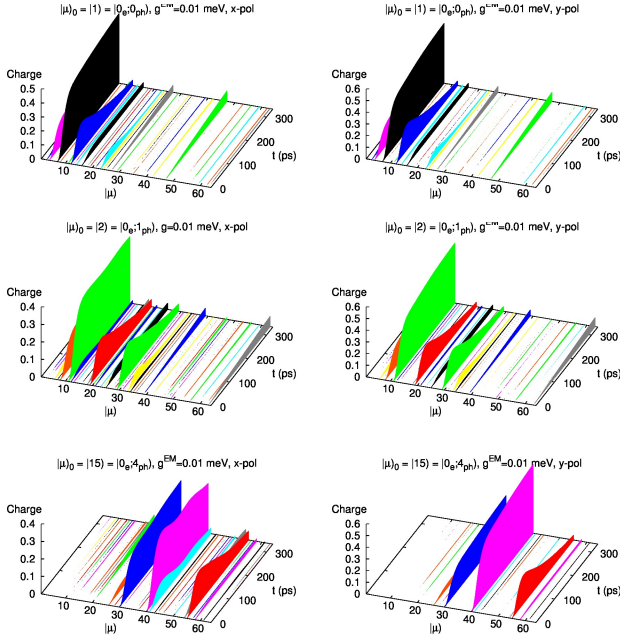


FIG. 6. (Color online) The mean number of electrons $\langle N_e(t) \rangle$ in a MBS $|\mu\rangle$ for x -polarization (left) and y -polarization (right) as a function of time. Initially, at $t = 0$, there is no photon in the cavity (top panels), 1 photon (middle panels), or 4 photons (bottom panels). The initial number of electrons is zero in all cases. $B = 0.1$ T, $g^{\text{EM}} = 0.01$ meV, $\hbar\omega = 0.4$ meV, $\mu_L = 2.0$ meV, $\mu_R = 1.4$ meV, $\hbar\Omega_0 = 1.0$ meV, $\Delta_E^L = 0.25$ meV, $g_0^l a_w^{3/2} = 53.14$ meV, $\delta_{1,2}^l a_w^2 = 0.4916$, $L_x = 300$ nm, $m^* = 0.067m_e$, and $\kappa = 12.4$.

ber of photons $\langle N_{\text{ph}} \rangle$ for the two different values of the electron-photon coupling strength in Fig. 8. In both cases the mean number of photons does not vary much for the y -polarization. Larger deviations are seen for the x -polarization with shorter period oscillations for the stronger coupling.

Again, a better insight into the photon-electron dynamics can be gained by observing the evolution of the mean photon number of each MBS which is presented in Fig. 9 for the weaker coupling and in Fig. 10 for the stronger one. For both cases we notice the rapid decay of the photon number from their initial state if the number was initially 1 or larger. With reference and comparison to Fig. 2 we observe a fast build up of electron-photon many-body states with a considerable photon component and higher energy. The total number of photons does not change fast in the system, but the introduction of electrons to the system through the leads results in a fast redistribution of the photons into many-body states of quasiparticles, or in other words the preexisting initial photons participate in and facilitate the build up of many-body states with higher energy. The slow change in the total photon number in Fig. 8 reflects phenomena of radiation absorption and emission while the rapid change with time in the occupation in Figs 6 and 7 indicates the creation of quasiparticles with definite electron

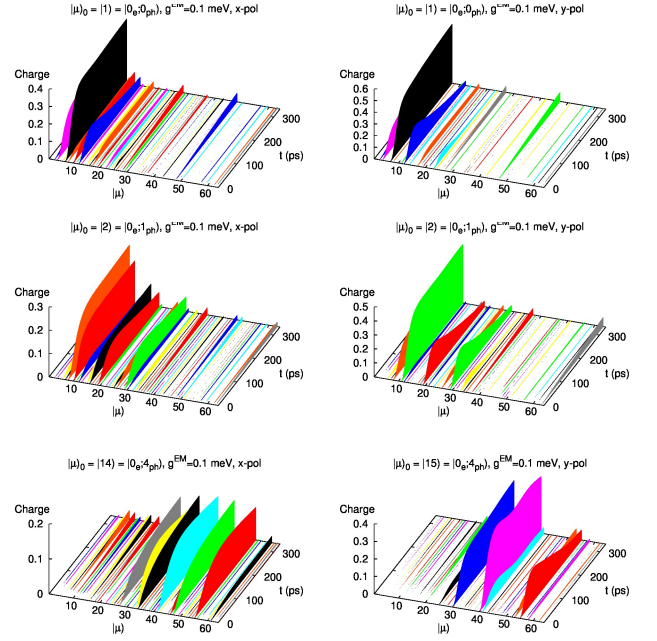


FIG. 7. (Color online) The mean number of electrons $\langle N_e(t) \rangle$ in a MBS $|\mu\rangle$ for x -polarization (left) and y -polarization (right) as a function of time. Initially, at $t = 0$, there is no photon in the cavity (top panels), 1 photon (middle panels), or 4 photons (bottom panels). The initial number of electrons is zero in all cases. $B = 0.1$ T, $g^{\text{EM}} = 0.10$ meV, $\hbar\omega = 0.4$ meV, $\mu_L = 2.0$ meV, $\mu_R = 1.4$ meV, $\hbar\Omega_0 = 1.0$ meV, $\Delta_E^L = 0.25$ meV, $g_0^l a_w^{3/2} = 53.14$ meV, $\delta_{1,2}^l a_w^2 = 0.4916$, $L_x = 300$ nm, $m^* = 0.067m_e$, and $\kappa = 12.4$.

and photon components. We thus observe phenomena on at least two different time scales.

We notice again (see Fig. 9) that for the weak electron-photon coupling there is not a large difference between the two polarizations except in the case of no initial photon.

It is well known that the GME in the approximation used here can lead to nonphysical negative probability for occupation of individual many-body levels if the coupling to the reservoirs is too strong.⁴² We have avoided this problem by keeping the coupling low enough. It is interesting to note here that it is our experience that after coupling to the photon system such a negative probability will first turn up in the probability for a photon occupation before it would be seen in the probability for the occupation of an electron.

The total current from the left lead into the system and from the system to the right lead is displayed in Figs 11 and 12 for both polarizations. The irregular short period oscillation seen in the current stems from addition of partial currents per each many-body state with simple almost harmonic oscillations of various short periods characteristic for each component. For the weak coupling, $g^{\text{EM}} = 0.01$ meV, and no photon present at $t = 0$ the left- and right currents are almost identical and very close to the current for the electron system with

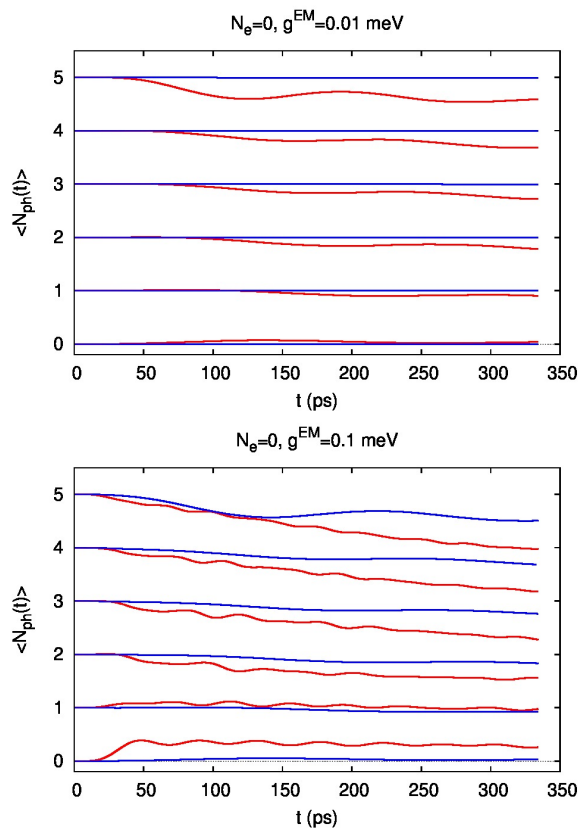


FIG. 8. (Color online) The total mean number of photons $\langle N_{\text{ph}} \rangle$ as a function of time for $g^{\text{EM}} = 0.01$ meV (upper panel) and $g^{\text{EM}} = 0.10$ meV (lower panel). x -polarization (red), and y -polarization (blue). $B = 0.1$ T, $\hbar\Omega_0 = 1.0$ meV, $\hbar\omega = 0.4$ meV, $\mu_L = 2.0$ meV, $\mu_R = 1.4$ meV, $L_x = 300$ nm, $\Delta_E^l = 0.25$ meV, $g_0^l a_w^{3/2} = 53.14$ meV, $\delta_{1,2}^l a_w^2 = 0.4916$, $m^* = 0.067m_e$, and $\kappa = 12.4$.

no coupling to cavity photons. This changes slightly for some photons initially present in the system, especially for $t \sim 300$ ps when the system is approaching a steady state. Here, we should mention that the photon energy, $\hbar\omega = 0.4$ meV, was selected to be smaller than the characteristic confinement energy in the y -direction and not to be in resonance with any Coulomb interacting MESs.

In the case of a stronger electron-photon coupling, $g^{\text{EM}} = 0.1$ meV, the charging of the central system is attenuated by the presence of x -polarized photons at $t = 0$. We are describing a central system here in the absence of any potential that can give its eigenstates different localization character, see Fig. 4, we do thus not expect any simple phenomena of photo enhanced conduction. The photon energy $\hbar\omega = 0.4$ meV is far from being in resonance with the characteristic energy for the y -confinement, but it is much closer to the characteristic energy for the x -direction. Inspection of the charge distribution of, or the occupation of many-body states $|\tilde{\mu}\rangle$ in Fig. 7 and the distribution of the photons in the same states in Fig. 10 demonstrates a strong correlation between the states and that the initial photons have

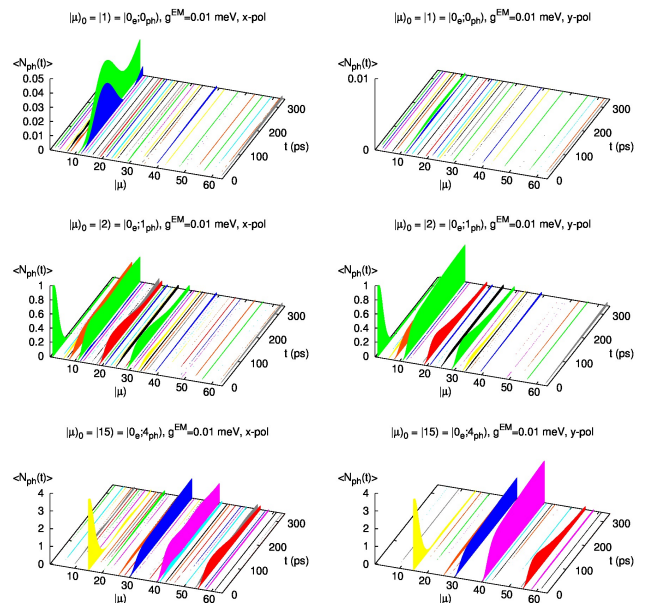


FIG. 9. (Color online) The mean number of photons $\langle N_{\text{ph}}(t) \rangle$ in a MBS $|\tilde{\mu}\rangle$ for x -polarization (left) and y -polarization (right) as a function of time. Initially, at $t = 0$, there are no photons in the cavity (top panels), 1 photon (middle panels), or 4 photons (bottom panels). $B = 0.1$ T, $g^{\text{EM}} = 0.01$ meV, $\hbar\omega = 0.4$ meV, $\mu_L = 2.0$ meV, $\mu_R = 1.4$ meV, $\hbar\Omega_0 = 1.0$ meV, $\Delta_E^l = 0.25$ meV, $g_0^l a_w^{3/2} = 53.14$ meV, $\delta_{1,2}^l a_w^2 = 0.4916$, $L_x = 300$ nm, $m^* = 0.067m_e$, and $\kappa = 12.4$.

caused the electrons to be distributed into many states. In a linear response situation which we do not have here we would say that the photon scattering of the electrons reduced the conduction. Here we have to say that the stronger photon-electron interaction for the case of the x -polarization attenuates the charging of the central system. Observation of the partial currents through the many-body state, not shown here, tells the same story. There are more states contributing to the charging, but they all bring less charge into the system. To understand this situation it is good to have in mind the similarity between the cavity photons here and confined phonons.

IV. SUMMARY

In this article we have taken the first steps to describe the transport of Coulomb interacting electrons through a photon cavity taking into account the geometry of the central system and the leads and allowing for a strong coupling to the photon mode. The central system is a parabolic quantum wire of finite length. Its aspect ratio and confinement characteristics make excitations for low values of the external magnetic field easier in the transport direction, the x -direction, than perpendicular to it, in the y -direction. By selecting the energy of the photon mode below the characteristic confinement frequency in

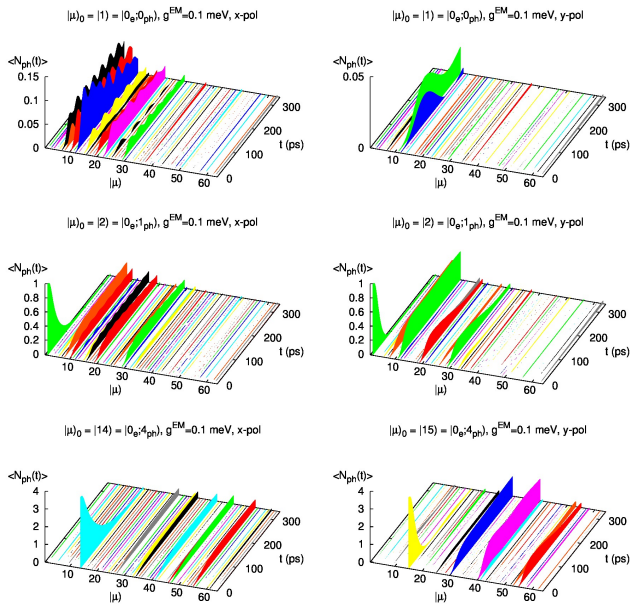


FIG. 10. (Color online) The mean number of photons $\langle N_{\text{ph}}(t) \rangle$ in a MBS $|\mu\rangle$ for x -polarization (left) and y -polarization (right) as a function of time. Initially, at $t = 0$, there are no photons in the cavity (top panels), 1 photon (middle panels), or 4 photons (bottom panels). $B = 0.1$ T, $g^{\text{EM}} = 0.10$ meV, $\hbar\omega = 0.4$ meV, $\mu_L = 2.0$ meV, $\mu_R = 1.4$ meV, $\hbar\Omega_0 = 1.0$ meV, $\Delta_E^l = 0.25$ meV, $g_0^l a_w^{3/2} = 53.14$ meV, $\delta_{1,2}^l a_w^2 = 0.4916$, $L_x = 300$ nm, $m^* = 0.067m_e$, and $\kappa = 12.4$.

the y -direction we demonstrate that the transport becomes very dependent on the polarization of the cavity mode and the number of photons initially present in the system at $t = 0$, before the electrons enter it. Generally, a higher initial photon number reduces the transient charging of the system with electrons. This effect is enhanced by increased coupling between the electrons and the photons. The largest reduction is found for several x -polarized photons in the system. The photon energy is then high enough to disperse the electrons into numerous excited states. The system does only contain delocalized electron states and this behavior has resemblance to reduced conductance due to phonon scattering of electrons. It has though to be kept in mind that we are observing a transient behavior here in the charging phase of the central system.

We observe dynamics on two different time scales here, the fast dispersion of electrons and photons into excited states initially seen in the transient regime, especially when analyzed for each many-body state, see Figs 6, 7, 9, and 10, and the slow decay or gain caused by radiation phenomena and reflected by the total number of photons in Fig. 8. Connected to the issue of the two time scales it is interesting to notice that in the case of no photon present in the system initially only many-body states with low energy and almost vanishing photon content are occupied by the electron entering the system. In

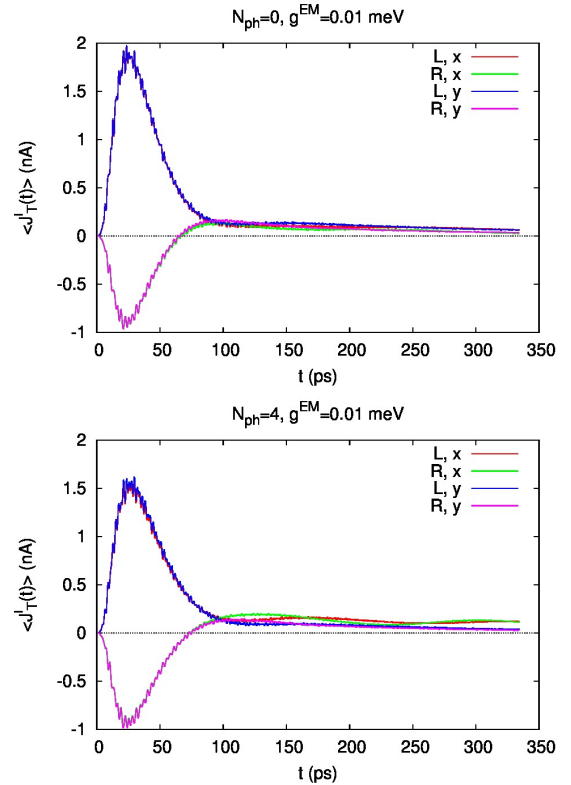


FIG. 11. (Color online) The total current from the left lead (L), and into the right lead (R) as a function of time for $g^{\text{EM}} = 0.01$ meV. Initially, at $t = 0$ there are no photons in the cavity (top panel), or 4 photons (bottom panel). $B = 0.1$ T, $\hbar\Omega_0 = 1.0$ meV, $L_x = 300$ nm, $\hbar\omega = 0.4$ meV, $\mu_L = 2.0$ meV, $\mu_R = 1.4$ meV, $\Delta_E^l = 0.25$ meV, $g_0^l a_w^{3/2} = 53.14$ meV, $\delta_{1,2}^l a_w^2 = 0.4916$, $m^* = 0.067m_e$, and $\kappa = 12.4$.

this situation the total photon content of the system only changes on the radiation time scale.

In the leads we have only electrons and in the central system quasiparticles with photon and electron content. Their lifetime is determined by the coupling to the leads and the time scale of radiation processes. The original coupling Hamiltonian of the leads and the central system, H_T , describes the entry or exit of noninteracting electrons to the central system from the leads. The two unitary transformations of H_T , first to the basis of interacting MESs and the second one to the electron-photon many-body basis guarantee that the coupling between the leads and the central system describes how electrons leave or enter the leads, and conversely how the number of quasiparticles or photons changes in the system. This stepwise introduction of complexity to the model, concurrent stepwise truncation of the ensuing Fock-space, and unitary transformation of the Hamiltonian at each step to the appropriate basis enables us to attack a problem that otherwise requires too large Fock space for numerical calculations. This procedure can still be streamlined in order to describe systems with stronger electron-photon coupling or more complex geometry.

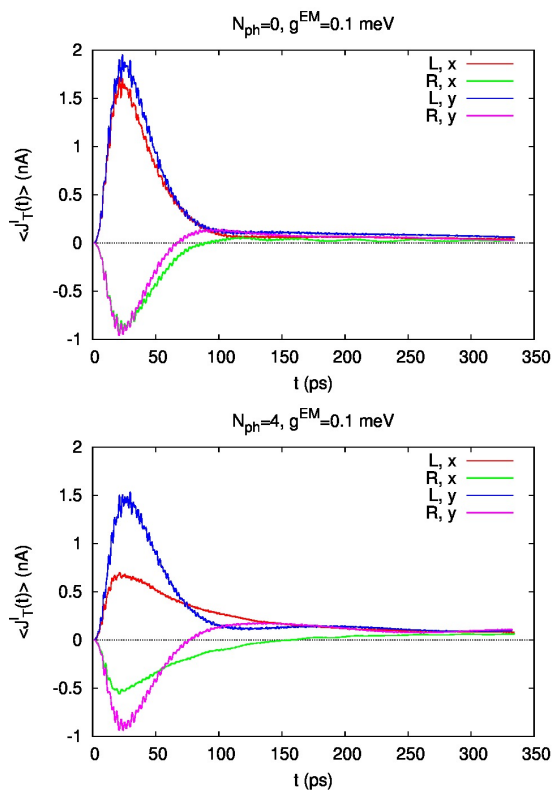


FIG. 12. (Color online) The total current from the left lead (L), and into the right lead (R) as a function of time for $g^{\text{EM}} = 0.1$ meV. Initially, at $t = 0$ there are no photons in the cavity (top panel), or 4 photons (bottom panel). $B = 0.1$ T, $\hbar\Omega_0 = 1.0$ meV, $L_x = 300$ nm, $\hbar\omega = 0.4$ meV, $\mu_L = 2.0$ meV, $\mu_R = 1.4$ meV, $\Delta E^l = 0.25$ meV, $g_0^l a_w^{3/2} = 53.14$ meV, $\delta_{1,2}^l a_w^2 = 0.4916$, $m^* = 0.067m_e$, and $\kappa = 12.4$.

The anisotropic response of the electron system to the two different polarizations of the photon field is caused by the confinement energy in the y -direction, $\hbar\Omega_0 = 1.0$ meV, being larger than both the photon energy, $\hbar\omega = 0.4$ meV, and the lowest excitation in the x -direction, $\Delta E_x \sim 0.2$ meV. At the low energy we are observing the properties of the system here it is much “harder”

or “stiffer” in the y - than the x -direction. We thus do not see much change in the properties of the system (see Fig. 11 and 12) varying the initial photon number or the coupling strength to the photons for the parameter range explored here. For the low coupling strength, $g^{\text{EM}} = 0.01$ meV there is not much difference either between the system properties for the two polarizations, but it is interesting to notice how similar the charging per MBS for the stronger coupling, $g^{\text{EM}} = 0.1$ meV, and y -polarization (see the right panels of Fig. 7) is to the charging at the weaker coupling and x -polarization (see the left panels of Fig. 6). The same analogy is found for the photon component in the MBS (compare the right panels of Fig. 10 to the left panels of Fig. 9). This analogy hints at a highly anisotropic “effective coupling” of the electrons and cavity photons for the geometry selected here.

The strong coupling of the electrons to the photon field leads to polarization effects in our system that require a large functional basis for the electron states of our system to describe correctly. This together with other important properties of the closed system will be discussed elsewhere³⁶ and is the limiting factor here in how strong coupling we can describe in our present system and still manage observation of the time evolution according to the GME.

ACKNOWLEDGMENTS

The authors acknowledge discussions with Ivan Shelykh and Valeriu Moldoveanu. The authors acknowledge financial support from the Icelandic Research and Instruments Funds, the Research Fund of the University of Iceland, the National Science Council of Taiwan under contract No. NSC100-2112-M-239-001-MY3. HSG acknowledges support from the National Science Council, Taiwan, under Grants No. 97-2112-M-002-012-MY3, and No. 100-2112-M-002-003-MY3, support from the Frontier and Innovative Research Program of the National Taiwan University under Grants No. 99R80869 and No. 99R80871, and support from the focus group program of the National Center for Theoretical Sciences, Taiwan.

* vidar@hi.is

† cstang@nuu.edu.tw

‡ goan@phys.ntu.edu.tw

¹ C. S. Tang and C. S. Chu, Phys. Rev. B, **60**, 1830 (1999).

² C. S. Tang, Y. H. Tan, and C. S. Chu, Phys. Rev. B, **67**, 205324 (2003).

³ G. Zhou and Y. Li, J. Phys.: Condens. Matter, **17**, 6663 (2005).

⁴ M. A. Zeb, K. Sabeeh, and M. Tahir, Phys. Rev. B, **78**, 165420 (2008).

⁵ C. H. Lin, C. S. Tang, and Y. C. Chang, Phys. Rev. B, **78**, 245312 (2008).

⁶ K. Torfason, C.-S. Tang, and V. Gudmundsson, Phys.

Rev. B, **80**, 195322 (2009).

⁷ D. Kienle and F. Léonard, Phys. Rev. Lett., **103**, 026601 (2009).

⁸ P. Myöhänen, A. Stan, G. Stefanucci, and R. van Leeuwen, Phys. Rev. B, **80**, 115107 (2009).

⁹ G. Stefanucci, E. Perfetto, and M. Cini, Phys. Rev. B, **81**, 115446 (2010).

¹⁰ N. R. Abdullah, C.-S. Tang, and V. Gudmundsson, Phys. Rev. B, **82**, 195325 (2010).

¹¹ M. Tahir and A. MacKinnon, Phys. Rev. B, **81**, 195444 (2010).

¹² P.-W. Chen, C.-C. Jian, and H.-S. Goan, Phys. Rev. B, **83**, 115439 (2011).

- ¹³ S. A. Gurvitz and Y. S. Prager, Phys. Rev. B, **53**, 15932 (1996).
- ¹⁴ N. G. van Kampen, *Stochastic Processes in Physics and Chemistry*, 2nd ed. (North-Holland, Amsterdam, 2001).
- ¹⁵ U. Harbola, M. Esposito, and S. Mukamel, Phys. Rev. B, **74**, 235309 (2006).
- ¹⁶ A. Braggio, J. König, and R. Fazio, Phys. Rev. Lett., **96**, 026805 (2006).
- ¹⁷ C. Emary, D. Marcos, R. Aguado, and T. Brandes, Phys. Rev. B, **76**, 161404(R) (2007).
- ¹⁸ A. Bednorz and W. Belzig, Phys. Rev. Lett., **101**, 206803 (2008).
- ¹⁹ V. Moldoveanu, A. Manolescu, and V. Gudmundsson, New Journal of Physics, **11**, 073019 (2009).
- ²⁰ V. Gudmundsson, C. Gainar, C.-S. Tang, V. Moldoveanu, and A. Manolescu, New Journal of Physics, **11**, 113007 (2009).
- ²¹ E. Vaz and J. Kyriakidis, Journal of Physics Conference Series, **107**, 012012 (2008).
- ²² V. Gudmundsson, C.-S. Tang, O. Jonasson, V. Moldoveanu, and A. Manolescu, Phys. Rev. B, **81**, 205319 (2010).
- ²³ M. Helm, *Intersubband Transitions in Quantum Wells: Physics and Device Applications I*, edited by H. C. Liu and F. Capasso (Academic Press, 2000).
- ²⁴ A. Gabbay, J. Reno, J. R. Wendt, A. Gin, M. C. Wanke, M. B. Sinclair, E. Shaner, and I. Brener, Appl. Phys. Lett., **98**, 203103 (2011).
- ²⁵ C. Ciuti, G. Bastard, and I. Carusotto, Phys. Rev. B, **72**, 115303 (2005).
- ²⁶ M. Devoret, S. Girvin, and R. Schoelkopf, Ann. Phys., **16**, 767 (2007).
- ²⁷ A. A. Abdumalikov, O. Astafiev, Y. Nakamura, Y. A. Pashkin, and J. Tsai, Phys. Rev. B, **78**, 180502(R) (2008).
- ²⁸ F. D. Zela, E. Solano, and A. Gago, Optics Communications, **142**, 106 (1997).
- ²⁹ A. T. Sornborger and A. N. C. M. R. Geller, Phys. Rev. A, **70**, 052315 (2004).
- ³⁰ E. K. Irish, Phys. Rev. Lett., **99**, 173601 (2007).
- ³¹ M. Delbecq, V. Schmitt, F. Parmentier, N. Roch, J. Viennot, G. Fève, B. Huard, C. Mora, A. Cottet, and T. Kontos, arXiv:1108.4371 (2011).
- ³² T. Frey, P. J. Leek, M. Beck, A. Blais, T. Ihn, K. Ensslin, and A. Wallraff, arXiv:1108.5378 (2011).
- ³³ S. Nakajima, Prog. Theor. Phys., **20**, 948 (1958).
- ³⁴ R. Zwanzig, J. Chem. Phys., **33**, 1338 (1960).
- ³⁵ V. Moldoveanu, A. Manolescu, C.-S. Tang, and V. Gudmundsson, Phys. Rev. B, **81**, 155442 (2010).
- ³⁶ O. Jonasson, arXiv:1109.4594 (2011).
- ³⁷ I. Magnúsdóttir and V. Gudmundsson, Phys. Rev. B, **60**, 16591 (1999).
- ³⁸ I. Magnúsdóttir and V. Gudmundsson, Phys. Rev. B, **61**, 10229 (2000).
- ³⁹ I. D. Feranchuk, L. I. Komarov, and A. P. Ulyanenko, J. Phys. A: Math. Gen., **29**, 4035 (1996).
- ⁴⁰ X.-H. Li, K.-L. Wang, and T. Liu, Chin. Phys. Lett., **26**, 044212 (2009).
- ⁴¹ J. Jin, X.-Q. Li, M. Luo, and Y. Yan, J. Appl. Phys., **109**, 053704 (2011).
- ⁴² R. S. Whitney, J. Phys. A: Math. Theor., **41**, 175304 (2008).